

Sensor trajectory estimation by triangulating lidar returns

Charles F. F. Karney* and Sujeong Kim†

SRI International, Princeton, NJ 08543-6449, USA

(Dated: August 25, 2022)

The paper describes how to recover the sensor trajectory for an aerial lidar collect using the data for multiple-return lidar pulses. This work extends the work of Gatziolis and McGaughey (2019) by performing a least-squares fit for multiple pulses simultaneously with a spline fit for the sensor trajectory. The method can be naturally extended to incorporate the scan angle of the lidar returns following Hartzell (2020). This allows the pitch and the yaw of the sensor to be estimated in addition to its position.

Keywords: airborne laser scanning; trajectory; aircraft position; simulation; pulse angle

1. INTRODUCTION

Lidar data sets, typically provided in the form of “las” files (ASPRS, 2019), often do not contain information on the location of the sensor platform as a function of time. For data sets which include the GPS time for each return, it is possible to identify the multiple returns originating from a given lidar pulse and thus determine its direction. By combining the data for multiple pulses emitted in a short time, it is possible to “triangulate” for the position of the sensor. This idea was proposed by Gatziolis and McGaughey (2019) who showed how to obtain a full sensor trajectory.

Here we reformulate this problem with a view to obtaining a more accurate trajectory. The trajectory is modeled as a cubic spline fit. Such a fit independently fits the x , y , and z components of $\mathbf{R}(t)$, the position of the sensor. The *unknowns* in this model are the parameters specifying the cubic splines. The *knowns* are the positions (and times) of the multiple returns from individual lidar pulses. The optimization problem is then to adjust parameters specifying the trajectory to minimize the mean squared error between the returns and a ray drawn from the sensor position to the mean position of the return. This is a rather complex nonlinear optimization problem. Fortunately, it is one that is easily handled by the software library Ceres Solver (Agarwal *et al.*, 2022).

Hartzell (2020) proposed using just the scan angles of the lidar returns to compute the lidar trajectory. This information does not constrain the trajectory as tightly as the multi-return data. However the framework offered by Ceres Solver is sufficiently flexible to allow the scan-angle data to be included in the optimization problem. This allows the trajectory to be estimated even in cases of sparse multiple returns. More importantly it allows the yaw and pitch of the sensor to be estimated.

2. FIXED SENSOR

In order to introduce the concepts, let us start first by assuming that the sensor is fixed and emits n multi-return pulses, indexed by $i \in [1, n]$. We shall only consider the first and last returns (ignoring any intermediate returns). We denote positions of the returns by

$$\mathbf{r}_i^\pm = \mathbf{r}_i \pm d_i \mathbf{p}_i. \quad (1)$$

Here \mathbf{r}_i^\pm are the positions of first and last returns, \mathbf{r}_i is their mean, \mathbf{p}_i is the unit vector in the direction from the last to the first return, and d_i is half the distance between the returns.

A. The reverse method

The goal now is to determine the position \mathbf{R} consistent with these returns. One approach is to consider the n rays

$$\mathbf{r}_i + s_i \mathbf{p}_i, \quad (2)$$

where the distance along the ray is parameterized by s_i and to solve the $3n$ equations

$$\mathbf{r}_i + s_i \mathbf{p}_i - \mathbf{R} = \mathbf{h}_i \approx 0 \quad (3)$$

for the $3 + n$ unknowns \mathbf{R} and s_i . This is an overdetermined system for 2 or more pulses and we can then use standard linear algebra methods to find the solution which minimizes $\sum_i h_i^2$, the so-called least-squares solution.

This is the approach used by Gatziolis and McGaughey (2019) who consider just pairs of pulses $n = 2$. The problem is that the resulting solution for \mathbf{R} is typically not the optimal solution for the trajectory problem because the system of equations does not involve the return separation d_i so pulses with closely separated returns are treated equally to pulses with widely separated returns. In reality, the latter returns should be weighted more heavily.

Gatziolis and McGaughey address this problem by selecting an *optimal* pair of returns based on the return separation and the angle between the pulses. This is based on a weighting function which needs to be separately estimated.

*Electronic address: charles.karney@sri.com;
ORCID: 0000-0002-5006-5836

†Electronic address: sujeong.kim@sri.com;
ORCID: 0000-0002-2641-395X

We use a simplified version of this linear least-squares problem to find an initial trajectory for our method described below. Using the z component of the residue equations to eliminate s_i from the system, the equations become

$$\begin{aligned} \left(r_{i,x} - \frac{p_{i,x}}{p_{i,z}} r_{i,z} \right) - \left(R_x - \frac{p_{i,x}}{p_{i,z}} R_z \right) &= h_{i,x} \approx 0, \\ \left(r_{i,y} - \frac{p_{i,y}}{p_{i,z}} r_{i,z} \right) - \left(R_y - \frac{p_{i,y}}{p_{i,z}} R_z \right) &= h_{i,y} \approx 0. \end{aligned}$$

We can write this as the explicit overdetermined linear system

$$\mathbf{A} \cdot \mathbf{R} - \mathbf{B} = \mathbf{H} \approx 0, \quad (4)$$

where \mathbf{A} is the $2n \times 3$ matrix

$$\mathbf{A} = \begin{pmatrix} \vdots & \vdots & \vdots \\ 1 & 0 & -p_{i,x}/p_{i,z} \\ 0 & 1 & -p_{i,y}/p_{i,z} \\ \vdots & \vdots & \vdots \end{pmatrix} \quad (5)$$

(two rows for each of the n pulses), \mathbf{B} is the $2n$ column vector

$$\mathbf{B} = \begin{pmatrix} \vdots \\ r_{i,x} - (p_{i,x}/p_{i,z})r_{i,z} \\ r_{i,y} - (p_{i,y}/p_{i,z})r_{i,z} \\ \vdots \end{pmatrix}, \quad (6)$$

and \mathbf{R} is the unknown sensor position.

This reduces the problem to $2n$ equations for 3 unknowns. In this formulation we determine the horizontal plane $z = R_z$ in which the rays are most tightly clustered. This is *not* the same problem as before; however with typical aerial lidar collects the two solutions for \mathbf{R} will be reasonably close. The difference is immaterial in our application since this solution for \mathbf{R} is only used as an initial estimate.

It's also possible to extend this method to allow the position of the sensor to be a function of time, for example,

$$\mathbf{R} = \mathbf{R}_0 + \mathbf{V}t.$$

The least-squares problem is now

$$\mathbf{A} \cdot \begin{pmatrix} \mathbf{R}_0 \\ \mathbf{V} \end{pmatrix} - \mathbf{B} = \mathbf{H} \approx 0, \quad (7)$$

where \mathbf{A} is now the $2n \times 6$ matrix

$$\mathbf{A} = \begin{pmatrix} \vdots & \vdots & \vdots & \vdots & \vdots & \vdots \\ 1 & 0 & -p_{i,x}/p_{i,z} & t_i & 0 & -t_i p_{i,x}/p_{i,z} \\ 0 & 1 & -p_{i,y}/p_{i,z} & 0 & t_i & -t_i p_{i,y}/p_{i,z} \\ \vdots & \vdots & \vdots & \vdots & \vdots & \vdots \end{pmatrix} \quad (8)$$

(and \mathbf{B} is unchanged). Here t_i is the time of the i th pulse.

Because pulses with widely separated returns constrain the possible position of the sensor more strongly than those with nearby returns, we multiply the rows in \mathbf{A} and \mathbf{B} associated

with the i th pulse by d_i , thereby appropriately *weighting* the least-squares problem.

As a practical matter, Eq. (7) can be solved to give \mathbf{R}_0 and \mathbf{V} by a suitable linear algebra package. For example, its solution can be obtained using Eigen (2021) with, for example,

$$\text{RV} = \mathbf{A}.\text{jacobiSvd}().\text{solve}(\mathbf{B});$$

B. The forward method

We term the above method of estimating \mathbf{R} described above the *reverse* method, because the rays are traced back from the returns to the sensor. An alternative is to trace the rays from \mathbf{R} to the midpoint of returns, the *forward* method. Thus each ray is given by

$$\mathbf{r}_i + s_i \hat{\mathbf{q}}_i, \quad (9)$$

where $\mathbf{q}_i = \mathbf{R} - \mathbf{r}_i$ and $\hat{\mathbf{q}}_i$ is the corresponding unit vector. The rays now all intersect at \mathbf{R} and the optimization problem is to find \mathbf{R} and s_i such that Eq. (9) is approximately equal to the position of the first return, \mathbf{r}^+ , from Eq. (1), i.e.,

$$d_i \mathbf{p}_i - s_i \hat{\mathbf{q}}_i = \mathbf{e}_i \approx 0. \quad (10)$$

Again we have $3n$ equations with $3 + n$ unknowns. However the quantities that are being minimized, \mathbf{e}_i , is the distance between the ray and the given positions of the returns. This method now naturally gives more weight to widely separated returns and the solution will similarly be more heavily governed by rays forming well-conditioned triangles.

Incidentally, the ray from \mathbf{R} to \mathbf{r}_i passes equally close to the first and last returns, so it is only necessary to minimize the distance to the first returns.

This system of equations is no longer linear, so it cannot be solved by linear algebra techniques. However, it is ideally suited for the Ceres Solver package. This finds the least-squares solution for nonlinear optimization problems. It also features

- Automatic determination of the Jacobian needed to find the solutions. This is achieved by writing the formulas in standard notation but with the variables declared to be the C++ type “Jet”. This combines a quantity and its derivative and, through overloaded operators and functions, follows all the standard rules of differentiation.
- A robust optimization. A standard problem of least-squares methods is that outliers in the data can skew the solution away from the “right” one. Ceres Solver includes a variety of “loss functions” which cause the effect of errors in the equations to fall off past some threshold. For example in this case, the threshold for the loss functions might be set to 0.01 m, the typical quantization error for positions in a `las` file.

C. Simplifying the forward method

We can simplify the problem by observing that \mathbf{e}_i is minimized with $s_i \approx d_i$ and that the resulting \mathbf{e}_i then spans a

two-dimensional space perpendicular to \mathbf{p}_i . Thus we can approximate the error \mathbf{e}_i by projecting the $\mathbf{R} - \mathbf{r}_i$ onto the plane perpendicular to \mathbf{p}_i at the first return. The first step is to convert to a primed coordinate system with \mathbf{r}_i at the origin and with the z' axis parallel to \mathbf{p}_i . This is achieved by the rotation matrix

$$\mathbf{M}_i = \begin{pmatrix} \frac{p_{i,x}^2 p_{i,z} + p_{i,y}^2}{p_{i,x}^2 + p_{i,y}^2} & \frac{-(1 - p_{i,z}) p_{i,x} p_{i,y}}{p_{i,x}^2 + p_{i,y}^2} & -p_{i,x} \\ -\frac{(1 - p_{i,z}) p_{i,x} p_{i,y}}{p_{i,x}^2 + p_{i,y}^2} & \frac{p_{i,x}^2 + p_{i,y}^2 p_{i,z}}{p_{i,x}^2 + p_{i,y}^2} & -p_{i,y} \\ p_{i,x} & p_{i,y} & p_{i,z} \end{pmatrix}. \quad (11)$$

This matrix rotates the coordinate system about the axis $\mathbf{z} \times \mathbf{p}_i$. Applying this translation and rotation to the sensor position gives

$$\mathbf{q}'_i = \mathbf{M}_i \cdot \mathbf{q}_i \quad (12)$$

Finally we project \mathbf{q}'_i onto the plane $z' = d_i$, which gives

$$\mathbf{e}'_i = \frac{d_i}{q'_{i,z}} \begin{pmatrix} q'_{i,x} \\ q'_{i,y} \end{pmatrix}. \quad (13)$$

Now the number of unknowns is just 3, the coordinates of \mathbf{R} , and the number of equations is $2n$, $\mathbf{e}_i \approx 0$ for each two-component vector \mathbf{e}_i

Solving this least-squares problem with Ceres Solver entails writing a C++ class implementing a “residue block”. The constructor for the class takes the *knowns* for a particular pulse, i.e., \mathbf{r}_i , \mathbf{p}_i , and d_i , and implements a function object which accepts the *unknowns* \mathbf{R} as input and returns the residue \mathbf{e}_i . This entails merely expressing the equations above as computer code. The problem is specified by n such residue blocks and an initial guess for \mathbf{R} (obtained, for example, by the reverse linear least-squares problem). Ceres Solver repeatedly invokes the function objects while adjusting \mathbf{R} to minimize $\sum e_i^2$. Because of the automatic differentiation built into Ceres Solver, it can compute the Jacobian for the problem which says how each component of \mathbf{e}_i changes as each component of \mathbf{R} is varied. This allows Ceres Solver to vary \mathbf{R} in an optimal way in its search for the least-squares solution.

3. THE TRAJECTORY COMPUTATION

The discussion above solves for the sensor position at a single instant of time. Of course, the sensor position is typically moving and it is convenient to model the motion as a cubic spline. One approach would be to perform a series of fixed sensor calculations, e.g., at 0.01 s intervals including for each calculation 10 pulses sampled at 0.001 s intervals and then to fit a spline to the resulting positions.

This approach has the drawback that some of the positions may be better approximated than others and the spline fit should respect this. This could be achieved by assigning weights to the various position estimated and this, essentially, is how Gatzliolis and McGaughey addressed this issue. However this put another layer of complexity into the problem.

In the spirit of Ceres Solver, it makes more sense to pose the entire exercise as a single least-squares problem. Let’s start by describing how to express a cubic spline.

A. The cubic spline

A cubic spline is a piece-wise cubic polynomial function which in our application we will use to approximate $\mathbf{R}(t)$. Each component of $\mathbf{R}(t)$ can be fit independently of the others. So we only need to consider a cubic spline for a scalar function $f(t)$ defined between T_0 and $T_K = T_0 + K \Delta t$. The time interval is divided into K blocks of duration Δt , with the k th block consisting of the interval $T_k \leq t < T_{k+1}$ where $T_k = T_0 + k \Delta t$ and $k \in [0, K)$. At internal block boundaries, $t = T_k$ for $k \in (0, K)$, we require that $f(t)$, $f'(t)$, and $f''(t)$ be continuous.

We shall specify the cubic polynomial for the k th block by the values of $f(t)$ and $g(t) = \Delta t f'(t)$ at the block boundaries. It is convenient to introduce a scaled centered time variable the block $\tau = (t - T_k)/\Delta t - \frac{1}{2}$. At the block boundaries, we have $f = f_k$ and $g = g_k$ at $\tau = -\frac{1}{2}$ and $f = f_{k+1}$ and $g = g_{k+1}$ at $\tau = \frac{1}{2}$. It is now a simple matter, e.g., by using the algebra system, Maxima (2022), to find the polynomial satisfying the boundary conditions

$$f(\tau) = a_0 + a_1 \tau + a_2 \tau^2 + a_3 \tau^3, \quad (14)$$

where

$$\begin{aligned} a_0 &= \frac{1}{8}(4f_+ - g_-), \\ a_1 &= \frac{1}{4}(6f_- - g_+), \\ a_2 &= \frac{1}{2}g_-, \\ a_3 &= -2f_- + g_+, \\ f_{\pm} &= f_{k+1} \pm f_k, \\ g_{\pm} &= g_{k+1} \pm g_k. \end{aligned}$$

By specifying the cubic polynomial by its values and derivatives at the block boundaries, we ensure continuity of $f(t)$ and $f'(t)$. The jump in the second derivative is given by

$$\Delta f''(T_k) = \frac{6(f_{k+1} - f_{k-1}) - 2(g_{k+1} + g_{k-1}) - 8g_k}{\Delta t^2}. \quad (15)$$

We will add $\Delta f''(T_k) \approx 0$ to the optimization problem.

In some situations, portions of a lidar collect might consist of “only returns”. These are, of course, not useful of determining the sensor trajectory by this method. If the stretch of such returns spans multiple blocks in the cubic spline, then the spline determination becomes badly conditioned. We address this by enforcing an *additional* constraint on the boundaries between two block with few multiple returns, namely that the third derivative is continuous. The jump in the third derivative is

$$\Delta f'''(T_k) = \frac{4f_k - 2(f_{k+1} + f_{k-1}) + (g_{k+1} - g_{k-1})}{\Delta t^3}. \quad (16)$$

In order to improve the smoothness of the trajectory, we add a constraint $\Delta f'''(T_k) \approx 0$ for all block boundaries. However, the weight for this constraint is very small except when the boundary separates blocks essentially devoid of multiple returns.

B. The optimization problem

We are now ready to set up the optimization problem for the entire trajectory. The knowns are t_i , \mathbf{r}_i , \mathbf{p}_i , and d_i for n pulses. These are the same as for the fixed sensor problem with the addition of the time t_i for each pulse. The unknowns are the sensor positions, $\mathbf{R}(t)$ and velocities, $\mathbf{R}'(t)$, at the block boundaries $t = T_k$ for $k \in [0, K]$.

The residue block for Ceres Solver now includes the time t_i . Each pulse is assigned to a particular time block and the constructor converts this time to the scaled time τ . The corresponding function object now takes the trajectory position and velocities at the block boundaries as input. It then uses the stored value of τ to evaluate the corresponding cubic polynomials for the 3 components of the sensor position $\mathbf{R}(t_i)$. The calculation then proceeds as in the fixed-sensor case and returns a two-component vector for the residue.

There is now also a new type of residue block to enforce the continuity of the acceleration at the internal block boundaries. The function object takes $\mathbf{R}(T_{k\pm 1})$, $\mathbf{R}'(T_{k\pm 1})$, and $\mathbf{R}''(T_k)$, and returns the jump in $\mathbf{R}''(T_k)$.

Overall there are $6(K + 1)$ unknowns (the positions and velocities at the block boundaries). The number of equations is $2n$ for the pulse residues, plus $3(K - 1)$ for the acceleration jump constraints, plus, optionally, another $3(K - 1)$ for the constraints on the jump in the third derivatives.

4. INCLUDING THE SCAN ANGLE DATA

The method outlined above depends on there being sufficient multiple returns present in the data. Hartzell (2020) suggested using the *scan angle* of the lidar pulse as an alternative method for triangulating the position of the sensor platform. This data can be seamlessly merged into our method allowing the sensor position to be estimated even in the absence of multiple returns. This has the added benefit that the attitude of the sensor platform can be estimated.

The scan angle of the lidar pulse is the angle measured rightwards from nadir of the lidar pulse as it sweeps left and right either side of the sensor platform. In some `las` formats, this is only recorded to the nearest whole degree.

We start by determining the direction of the laser pulse given the yaw ψ , pitch θ , and roll ϕ of the sensor platform and the scan angle α . The standard coordinate system is x east, y north, and z up. Given that the sensor starts in a reference orientation, level and heading due north, the sensor orientation is found by rotating by $+\phi$ about the y axis, followed by a rotation $+\theta$ about the x axis, followed by a rotation $-\psi$ about the z axis. In the reference orientation, the lidar pulse is emitted a direction obtained by rotating the downward vector by $-\alpha_i$

about the y axis (thus positive α_i is to the right of the sensor path). Taking account of the attitude of the sensor platform, the direction of the pulse is

$$\mathbf{N}(-\psi\hat{\mathbf{z}}) \cdot \mathbf{N}(+\theta\hat{\mathbf{x}}) \cdot \mathbf{N}(-\alpha_i\hat{\mathbf{y}}) \cdot (-\hat{\mathbf{z}}), \quad (17)$$

where $\mathbf{N}(\mathbf{n})$ is the matrix giving a right-handed rotation by $|n|$ about the axis $\hat{\mathbf{n}}$. Note that α_i includes both the roll of the sensor platform ϕ and the deflection of the lidar pulse relative to the sensor platform; so ϕ does not appear here.

Now consider a lidar pulse emitted with the sensor positioned at \mathbf{R} and the lidar return recorded at \mathbf{r}_i with scan angle α_i , so that the ray from the sensor to the return is $-\mathbf{q}_i = \mathbf{r}_i - \mathbf{R}$. We now reverse the order of rotations in Eq. (17) to put this ray back in a nominal reference frame for the lidar pulse,

$$\mathbf{q}_i'' = \mathbf{N}(+\alpha_i\hat{\mathbf{y}}) \cdot \mathbf{N}(-\theta\hat{\mathbf{x}}) \cdot \mathbf{N}(+\psi\hat{\mathbf{z}}) \cdot (-\mathbf{q}_i). \quad (18)$$

We require that \mathbf{q}_i'' be nearly parallel to the downward direction $-\hat{\mathbf{z}}$; or, equivalently, that the horizontally projected 2-vector

$$\mathbf{a}_i = \frac{1}{q_{i,z}''} \begin{pmatrix} q_{i,x}'' \\ q_{i,y}'' \end{pmatrix} \quad (19)$$

be close to zero.

The components of projected vector \mathbf{a}_i are in the reference frame of the sensor; thus the x component reflects an error in the given scan angle α_i , while the y component reflects an error in the unknown pitch θ . Because the recorded data for α_i often includes the rather large quantization error of 1° , we might wish to weight the y component of \mathbf{a}_i more heavily.

The conditions $\mathbf{a}_i \approx 0$ are just other constraints we can add to our optimization problem for Ceres Solver.

5. IMPLEMENTATION AND TESTING

The solution developed above was implemented as a filter of the Point Data Abstraction Library (Butler *et al.*, 2021; PDAL Contributors, 2022). It has subsequently incorporated into the PDAL source code repository (2022) as a possible ‘‘trajectory’’ filter. The input should be a `las` file for an aerial lidar collect including the GPS time, return number, and the scan angle. The filter produces a sensor trajectory (position and orientation) sampled at regular intervals. The internal parameters that govern the operation of the filter together with their default values and a brief description are given in Table 1.

Multiple returns are assumed to originate from the same lidar pulse if the times match. The filter combines the multi-return and the scan-angle constraints as follows: the sequence of pulses is broken into time intervals δt_r , resp. δt_s , for multi-return, resp. scan-angle, constraints and the ‘‘best’’ pulse is selected for each type of constraint. For multi-return constraints, this is the pulse with the largest separation between first and last returns. For scan-angle constraints, the midpoint of a run of pulses with the same scan angle is chosen (to minimize the effect of quantizing the scan angle to a whole degree in `las`

TABLE 1 Parameters used in the trajectory estimation code. The correspondence between these parameters and the notation in the paper is: $\delta t_r = \text{dtr}$, $\delta t_s = \text{dts}$, $t_r = \text{multiweight}$, and $w_s = \text{scanweight}$.

```

dtr = 0.005           # sampling interval multi-return (s) (inf = don't)
dts = 0.005           # sampling interval scan-angle (s) (inf = don't)
tblock = 1            # block size for cubic spline (s)
dr = 0.01             # error in returns (m)
dang = 1              # error in scan angle (deg)
scanweightest = 0.01  # relative weight for scan pulses in initial est
multiweight = 5        # weight for multi-return pulses in ceres problem
scanweight = 0.005    # weight for scan pulses in ceres problem
fixedpitch = nan      # fixed pitch value (deg) (nan = don't fix)
pitchweight = 1        # weight pitch vs scan angle
flipscanang = f        # does sign of scan angle need flipping
minsep = 0.5          # min separation (m) of returns considered
accelweight = 0.5      # weighting for acceleration constraint
clampweight = 0.0001  # weighting for general clamping constraint
straddleweight = 0.0001 # weighting for straddling clamping constraint
attaccelweight = 0.01 # weighting for acceleration constraint on attitude
attclampweight = 0.0001 # weighting for clamping constraint on attitude
extrapitchclamp = 1   # extra clamping for pitch component of attitude
vlevel = 0            # verbosity level
estn = 20              # min number of pulses to use of rough estimate
niter = 50             # number of iterations for ceres-solver
# used by the outside
tout = 0.01           # interval (s) for the reported trajectory

```

TABLE 2 Parameters used in the figures and the resulting discrepancies. Discrepancies are computed over the full trajectory (of duration 70 s) and are reported as mean \pm standard deviation.

	Fig. 1	Fig. 2	Fig. 3
δt_r (s)	0.005	∞	0.005
δt_s (s)	∞	0.005	0.005
w_r	5	—	5
w_s	—	5	0.005
ΔR_x (m)	0.02 ± 0.01	1.65 ± 2.22	same as Fig. 1
ΔR_y (m)	0.02 ± 0.01	-1.18 ± 0.21	”
ΔR_z (m)	-0.05 ± 0.05	-4.70 ± 0.50	”
$\Delta \theta$ ($^\circ$)	—	-0.20 ± 0.23	-0.05 ± 0.06
$\Delta \psi$ ($^\circ$)	—	0.27 ± 0.02	0.21 ± 0.08

files). In addition, weights, w_r and w_s , can be specified separately for the multi-return and scan-angle constraints. In this way it is easy to run with just multi-angle or just scan-angle constraints or some mixture of constraints.

Our test data was collected by the National Center for Airborne Laser Mapping (NCALM) in 2017 over the University of Houston. The data is given in UTM coordinates (zone 15n) and height above the ellipsoid. The direction was approximately westerly with northing 3 289.5 km and easting ranging from 276.3 km to 271.5 km, i.e., covering about 4.8 km in 70 seconds. We also had access to the smoothed best estimate of trajectory, SBET, for this collect. This serves as the ground truth for the trajectory.

We ran the trajectory estimation code with three different settings of the parameters as described in Table 2. Also shown in this table are the discrepancies in position $\Delta \mathbf{R} = \mathbf{R}_{\text{est}} - \mathbf{R}_{\text{sbet}}$, in pitch $\Delta \theta = \theta_{\text{est}} - \theta_{\text{sbet}}$, and in yaw $\Delta \psi = \psi_{\text{est}} - \psi_{\text{sbet}}$. The results are also shown graphically in Figs. 1–3. We estimate the trajectory of the entire 70 s trajectory; in these figures, we only display the data for the central 30 s of the flight.

In the first test, we included just multi-return data by setting $\delta t_s = \infty$; the estimated trajectory is based on the ideas of Gatzolis and McGaughey (2019), albeit using a considerably more sophisticated optimization strategy. Even though this involves a system of tens of thousands of equations, Ceres Solver handles it without difficulty in about 5 seconds of CPU time. The results are shown in Fig. 1 which shows that the estimated trajectory is within a few centimeters of the ground truth. On the one hand, this estimate is extraordinarily good; given that the lidar points are given only to the nearest centimeter, it’s difficult to envision doing substantially better than this. On the other hand, perhaps the good fit is unsurprising since, after all, we are just “undoing” the calculation that converted the raw data from the lidar unit in the points in the `las` file.

The next test, Fig. 2, switches to using only scan-angle constraints. This is an elaboration of the method proposed by Hartzell (2020). The use of these constraints allow us to estimate the pitch and yaw of the sensor, in addition to the position. We see that the estimated values for these components of the orientation faithfully track the ground truth data. However the discrepancy in the position is considerably worse (measured in meters instead of centimeters) than with using

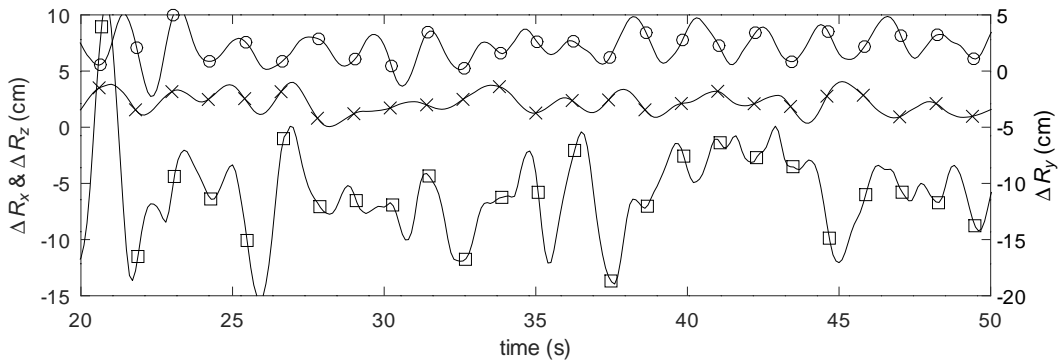


FIG. 1 The discrepancy in the estimated trajectory based only on multi-return constraints. The curves give the x , y , z components of $\Delta\mathbf{R}$ marked with crosses, circles, and squares respectively. Note well, the scale for ΔR_y is on the right.

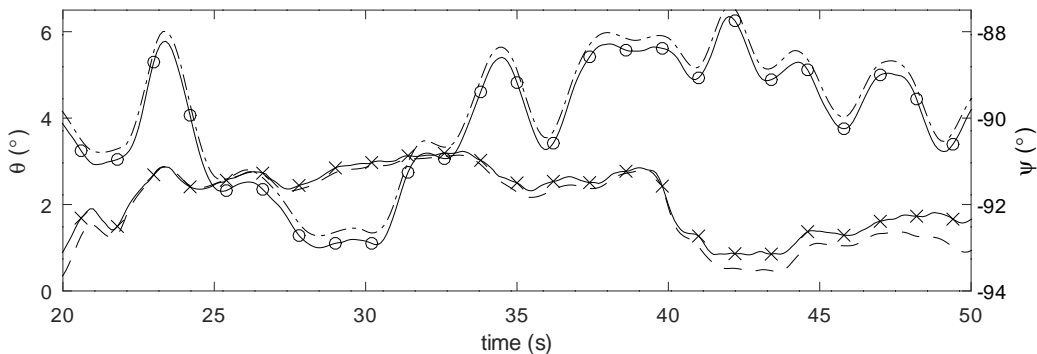


FIG. 2 The pitch and yaw of the sensor using only scan-angle constraints. The solid curves show the pitch θ (marked with crosses) and yaw ψ (marked with circles). The dashed and dot-dashed curves show the corresponding estimates. Note well, the scale for ψ is on the right

just the multi-return constraints; see the middle column of Table 2. This arises because the scan-angle constraints are ill-conditioned—a change in pitch can be compensated by a corresponding shift in position along the line of travel; note that largest variances in this case are in ΔR_x (the direction of travel) and $\Delta\theta$.

In the final test, Fig. 3, we include both multi-return and scan-angle constraints. Because we weight the multi-return constraints much more heavily, $w_r = 1000w_s$, the estimated position is the same as Fig. 1. The accurate position estimate then results in a much better estimate for θ compared to Fig. 2.

6. DISCUSSION

The method we have described for recovering the sensor trajectory for lidar data in a `las` file provides accurate results for both the position and the orientation (yaw and pitch) of the sensor. It incorporates the triangulation method using multi-return pulses of Gatzolis and McGaughey (2019) and the triangulation method using the scan-angle of pulses of Hartzell (2020). However in both cases, our method offers a more robust estimation of the trajectory by performing a single optimization for the spline fit for the sensor trajectory. One important aspect of this optimization is that it au-

tomatically accounts for the conditioning of the triangulation naturally weighting well-conditioned triangles more heavily.

The example data set we used was for a relatively short flight, with a dense coverage of returns throughout the flight; approximately one quarter of the lidar pulse resulting in multiple returns. The data for longer flights might need to be broken into shorter sequences for processing and our method could easily be adapted to ensure a continuous spline fit throughout the entire flight. Data collects with large breaks in the returns, e.g., from flying over water, would need to be divided at the breaks. Similarly, we should expect the performance to degrade with collects giving returns from just one side of the aircraft, e.g., when flying along a coast, and collects over terrain resulting in a small fraction of multiple returns.

When discussing the results, we were careful to call the difference between the estimated trajectory and the ground truth the “discrepancy”. This encompasses the irreducible errors because the `las` data includes quantization errors (typically 1 cm for position and 1° for the scan angle). In addition, there will be systematic errors because we treated UTM coordinates plus height as a Euclidean coordinate system. This ignores the fact that $z = 0$ is not flat, the scale of the horizontal dimension is not unity (leading to errors in the height estimate), and the meridian convergence (leading to errors in the estimate of the yaw). However, disentangling these errors from pos-

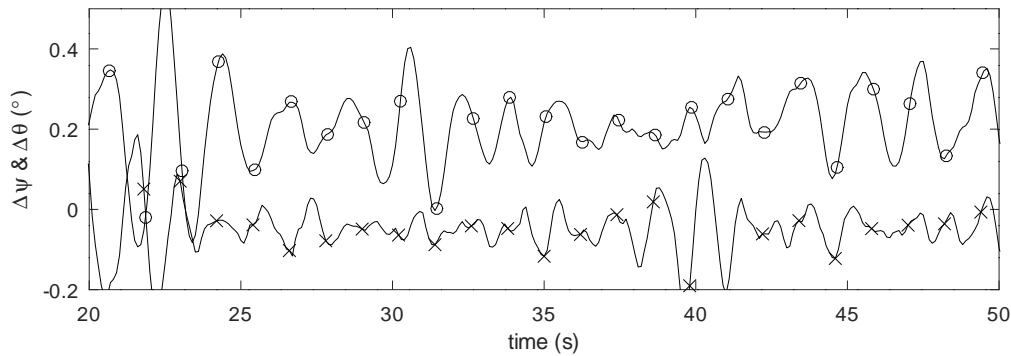


FIG. 3 The discrepancies in the pitch (marked with crosses) and yaw (marked with circles) when multi-return and scan-angle constraints are used.

sible lever arm contributions because of an offset in the inertial navigation unit and the lidar sensor would require detailed knowledge of the lidar configuration for our test collect and the post-processing required in producing the `las` file. Given that the discrepancies, a few centimeters for position and a fraction of a degree for orientation, are within the expected bounds given the errors in `las` data, pursuing other sources of the discrepancy would require analysis of a broader range of test data.

Supplementary materials

The following supporting data is provided in the `anc` directory in the source package on arXiv: original lidar point cloud from NCALM (with the intensity field removed and compressed), `C2_L2.laz`; SBET data (trimmed for this collect), `sbet_047_IGS08-UTM15N-Ellipsoid-trim.txt`; our trajectory estimate (using the parameters of Fig. 3), `C2_L2-traj3.txt`.

Funding

This material is based upon work supported by the United States Army Engineer Research and Development Center (ERDC) under contract FA2487-21-F-1103. The tests described and the resulting data presented herein, unless otherwise noted, are supported under PE 0602146A “Network C3I Technology,” Project AT7 “Network-Enabled Geospatial GEOINT Services Tech” Task SAT701, 3D Terrain Automated Geospatial Co-Registration and Change Detection Algorithms. Any opinions, findings and conclusions or recommendations expressed in this material are those of the authors and do not necessarily reflect the views of the United States Army.

Acknowledgments

The authors thank Demetrios Gatzolis for providing source code for his algorithms, Ryan Villamil for pro-

ducing the resulting trajectories using the method of Gatzolis and McGaughey (2019), and Preston Hartzell for supplying his code for the scan-angle method. The test data for this study was provided by Craig Glennie and Preston Hartzell of the University of Houston.

References

- S. Agarwal, K. Mierle, and The Ceres Solver Team, 2022, *Ceres Solver, version 2.1*, URL <https://github.com/ceres-solver/ceres-solver>.
- ASPRS, 2019, *LAS specification 1.4–R14*, Technical report, The American Society for Photogrammetry & Remote Sensing, URL https://www.asprs.org/wp-content/uploads/2019/03/LAS_1_4_r14.pdf.
- H. Butler, B. J. Chambers, P. J. Hartzell, and C. L. Glennie, 2021, *PDAL: An open source library for the processing and analysis of point clouds*, *Computers and Geosciences*, **148**, 104680, doi:10.1016/j.cageo.2020.104680, URL <https://pdal.io>.
- Eigen, 2021, *a C++ template library for linear algebra: matrices, vectors, numerical solvers, and related algorithms, version 3.4*, URL <https://eigen.tuxfamily.org>.
- D. Gatzolis and R. J. McGaughey, 2019, *Reconstructing aircraft trajectories from multi-return airborne laser-scanning data*, *Remote Sensing*, **11**(19), 2258, doi:10.3390/rs11192258.
- P. J. Hartzell, 2020, *Airborne lidar sensor trajectory estimation from LAS scan angle field*, URL <https://github.com/pjhartzell/scan-angle.git>.
- Maxima, 2022, *A computer algebra system, version 5.46.0*, URL <https://maxima.sourceforge.io>.
- PDAL Contributors, 2022, *PDAL, version 2.4.3*, doi:10.5281/zenodo.6968095.
- PDAL source code repository, 2022, *Pull request #3743*, URL <https://github.com/PDAL/PDAL/pull/3743>.